Supporting Information

A Smartphone-Assisted Robust Sensing Platform for On-Site Quantitation of 2, 4-Dichlorophenoxyacetic Acid Using Red Emissive Carbon Dots

Dandan Su[a, 1], Xiaosong Han[b, 1], Xu Yan[a,], Rui Jin[a], Hongxia Li[c], Deshuai Kong[a], Hao Gao[b], Fangmeng Liu[a], Peng Sun[a], Geyu Lu[a, *]*

[a] *State Key Laboratory of Integrated Optoelectronics, College of Electronic Science and Engineering, Jilin University, Changchun 130012, People's Republic of China*

[b] *College of Computer Science and Technology, Jilin University, Changchun 130012, China*

[c] *Department of Food Quality and Safety, College of Food Science and Engineering, Jilin University, Changchun 130062, People's Republic of China*

***Corresponding Author**

E-mail Address: yanx@jlu.edu.cn

1 Dandan Su and Xiaosong Han contributed equally to this work

Table of content

Supporting Materials and Methods

Materials and Apparatus

Alkaline phosphatase (ALP), ascorbic acid-2-phosphate trisodium salt (AAP), ascorbic acid (AA) and cobaltous chloride ($CoCl_2 \cdot 6H_2O$), N, N-Dimethylformamide (DMF, ≥ 99.9%) were obtained from Sigma-Aldrich Corporation. Urea, citric acid, chlorite (NaClO), sodium hydroxide (NaOH) and hydrochloric acid (HCl) were obtained from Beijing Dingguo Changsheng Biotechnology Co. Ltd. Pesticides were bought from Tianjin Zhongyi Jiaxin Technology Development Co. Ltd.

The microstructures were recorded using JEM-2100 transmission electron microscope (TEM). Atomic force microscopy (AFM) (Dimension Icon, Bruker, Germany) was employed to characterize the height of materials. X-ray diffraction (XRD) analysis was used a Bruker AXS D8 Advance Powder X-ray diffractometer. X-ray photoelectron spectroscopy (XPS) was performed on an ESCALAB 250 XI electron spectrometer (Thermo). FT-IR spectra were recorded with Nicolet 6700 FT-IR spectrometer (Thermo). Fluorescence data were carried out by RF-5301 fluorescence spectrophotometer. UV-vis absorption spectra were recorded by UV-2550 spectrometer (Shimadzu).

Synthesis of CoOOH Nanosheets

3.0 mL of NaOH (1.0 mol L^{-1}) and 10.0 mL of $CoCl_2$ (10 mmol L^{-1}) were mixed and then sonicated for 2 min. Following, 500 μL of NaClO (0.9 mol L^{-1}) was injected and sonicated for another 15 min. The precipitate collected after centrifugation for 5 min at 6,000 r min^{-1} were washed with deionized water for several times. Finally, CoOOH nanosheets were freeze-dried to obtain a brown black powder.

Real Samples Detection

Real samples including lake water, pear juice, human urine and serum served as research targets to verify practical applications of the smartphone-connected sensor.

The lake water sample (10 mL) was filtered through a 0.22 mm membrane. Pear juice processed by juicer was extracted from commercial pears. The spiked samples were mixed with 10.0 mL acetonitrile and ultrasound for 5 min. After centrifuged twice at 10,000 rpm for 10 min, the

supernatant was collected. The supernatant was concentrated to 1 mL and diluted 10-fold to measure 2, 4-D according the mentioned process. For recovery study, certain amounts of 2, 4-D standard (0.1, 0.5, 1.0, 5.0 mg L^{-1}) were spiked into the samples before pretreatment and then evaluated by described procedure.

Human blood sample was collected from human volunteers through venipuncture at the China-Japan Union Hospital of Jilin University. The experiments were carried out in compliance with the relevant laws and institutional guidelines. Due to high protein in the blood plasma, some pretreatments were taken to eliminate the coexisting substances interferences. 1 mL of human serum was mixed with 2 mL of DI water and 2 mL of acetonitrile by vertexing for 5 min. Subsequently, the human serum sample was deproteinized by adding 5 mL of 10% (w/v) trichloroacetic acid. Finally, the serum solution was obtained by centrifuging (10,000 rpm, 15 min) to remove the protein precipitate and other large molecules. The supernatant serum samples were diluted 5-fold and applied to measure 2, 4-D according the mentioned process. For recovery study, certain amounts of 2, 4-D standard (0.1, 0.5, 1.0, 5.0 mg L^{-1}) were spiked into the samples and then evaluated by described procedure.

Human urine sample was obtained from a healthy volunteer. 1 mL of human urine was mixed with 2 mL of DI water and 2 mL of acetonitrile by vertexing for 5 min. Sample was centrifuged at 10000 rpm for 15 min and then diluted 10 times before use. Then the sample was applied to measure 2, 4-D according the mentioned process. For recovery study, certain amounts of 2, 4-D standard (0.1, 0.5, 1.0, 5.0 mg L^{-1}) were spiked into the samples and then evaluated by described procedure.

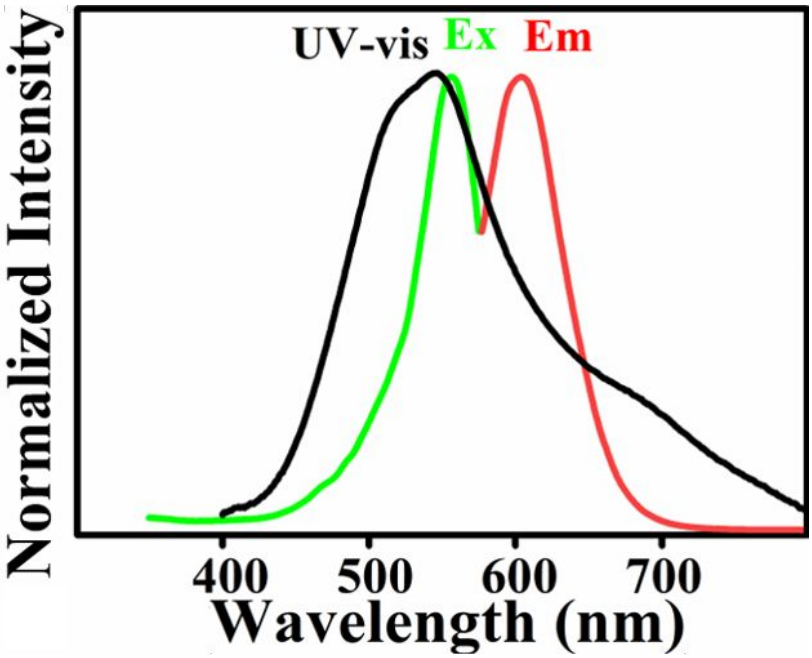

Figure S1. The UV-Vis, FL excitation (Ex) and FL emission (Em) spectra of CDs.

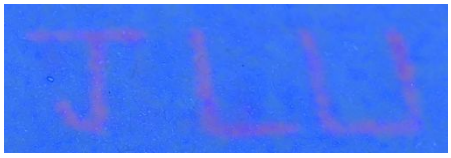

Figure S2. The red character “JLU” under the excitation wavelength of 365 nm.

Determination of Quantum Yield (QY)

The fluorescence quantum yields of CDs were using the following equation:

$$\Phi = \Phi' \times \frac{A'}{I'} \times \frac{I}{A} \times \frac{n^2}{n'^2}$$

where as Φ is QY of the CDs, I is the integrated FL intensity of CDs, n is the solvent refractive index (1.36 for ethanol) and A represent the optical density, respectively. The superscript " ' " indicated the reference data. For achieving the precious results, various concentrations of CDs and referenced samples were adjusted the absorption below 0.10.

	CDs				Rhodamine 6G			
Absorbance	**0.015**	**0.022**	**0.041**	**0.053**	**0.010**	**0.019**	**0.035**	**0.049**
Integrated FL intensity	**272**	**458**	**876**	**1050**	**2695**	**5079**	**8315**	**12760**
Slope	**20610**				**251167**			
QY	**7.8%**				**95%**			

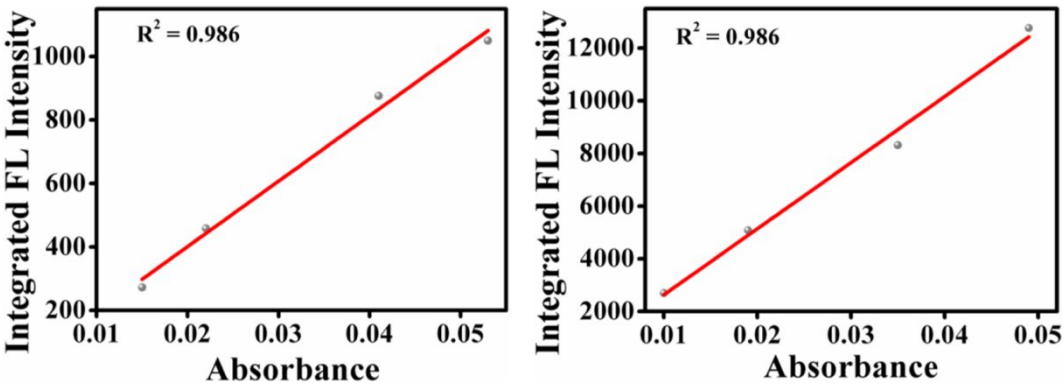

Figure S3. Plots of Integrated FL intensity of CDs and Rhodamine 6G as the function of optical absorbance at 530 nm.

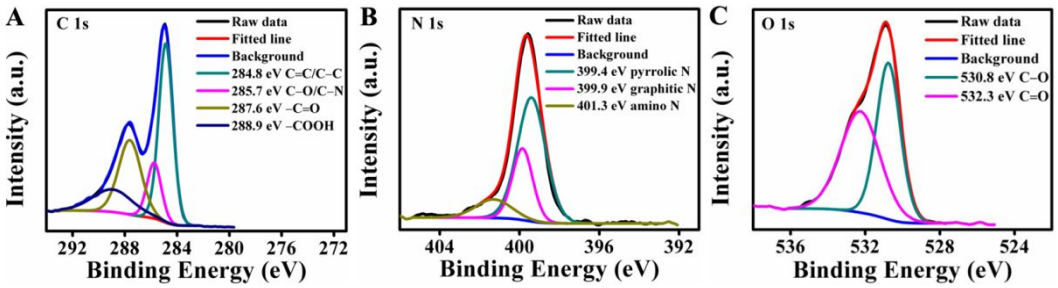

Figure S4. High-resolution (A) C 1s, (B) N 1s and (C) O 1s XPS spectra of CDs.

Stability Performance Studies of CDs

For evaluating pH stability, the FL intensity of CDs is collected under a series of pH values in the range of 5.8-8.8. Figure S5 revealed merely change of CDs, showing higher pH stability. Subsequently, thermal stability performance in Figure S6 demonstrated that CDs hold almost constant under the temperature range from 4-95 ^{o}C. The chemical stability under different chemical substance was also investigated explored. In Figure S7-8, the normalized FL intensity was almost the same in the presence of NaCl (0-200 mmol L^{-1}) and displayed good tolerance ability towards H_2O_2 even in high concentration of 5.0 mmol L^{-1}, indicating satisfied chemical stability of CDs. For photostability behavior, time course scan curve of CDs was obtained when 555 nm exciting for 60 min. Besides, we utilized an intensive xenon lamp for continuous excitation for 40 min and collected fluorescence intensity of CDs. In Figure S9, the fluorescence emission intensity of CDs preserved ~65% of the initial intensity after 40 min of xenon lamp irradiation (17 W/cm^2), indicating that the CDs possessed good photostability.

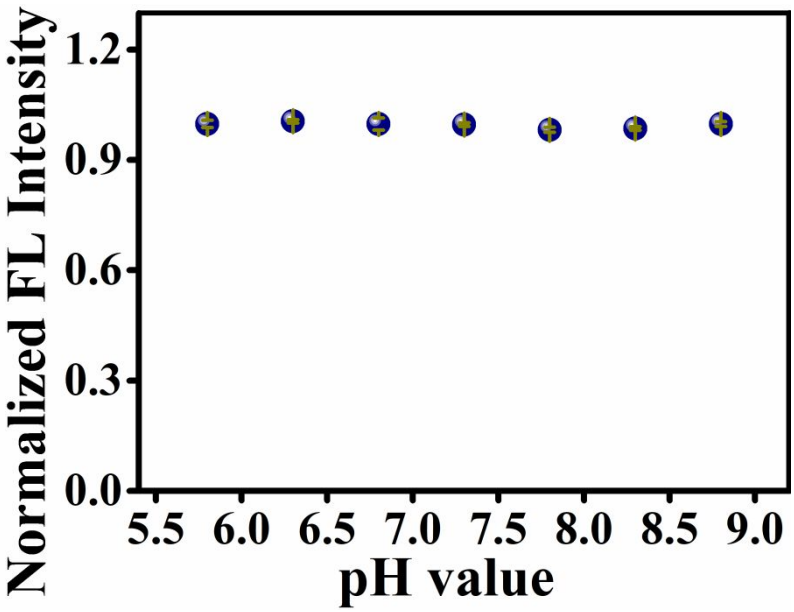

Figure S5. pH stability of CDs in the range of 5.8-8.8.

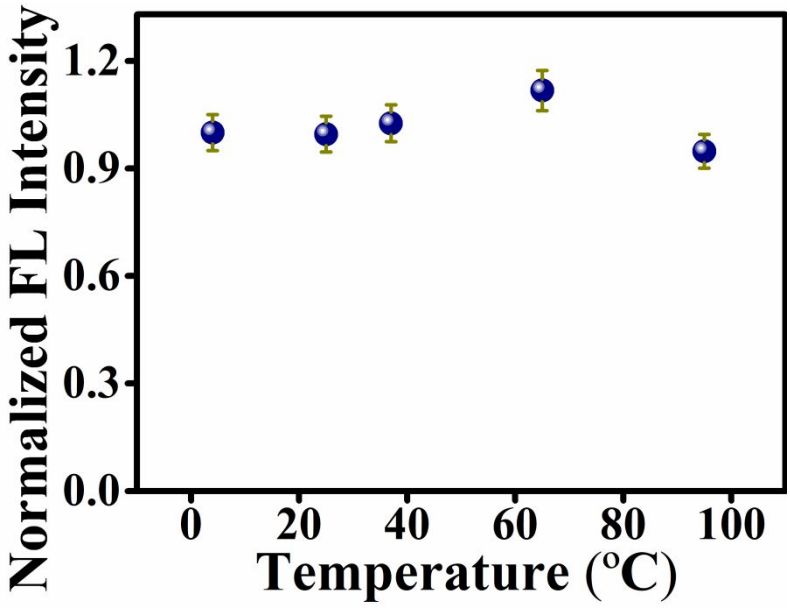

Figure S6. Thermal stability of CDs in the range of 4-95 °C. The FL intensity was obtained after reaction for 60 min in different temperatures (4, 25, 37, 65, 95 °C).

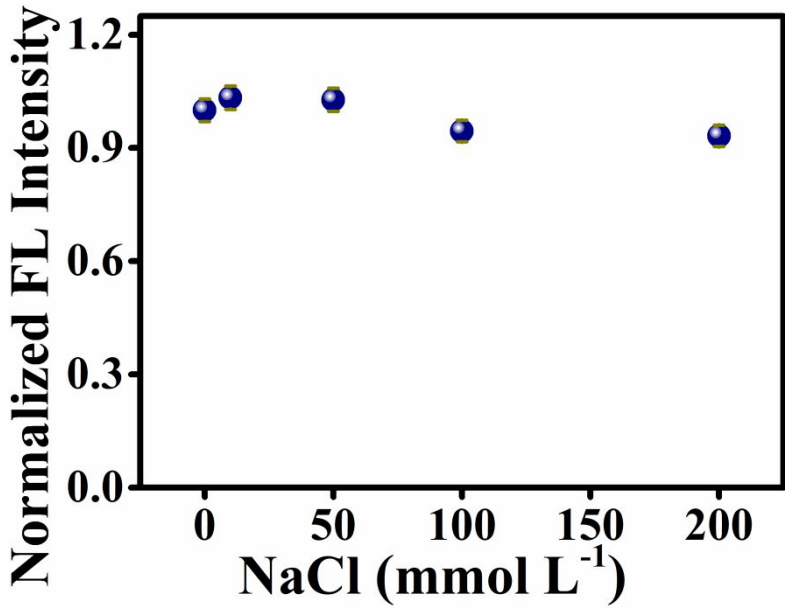

Figure S7. Salt stability of CDs in the presence of 0-200 mmol L^{-1} NaCl solution.

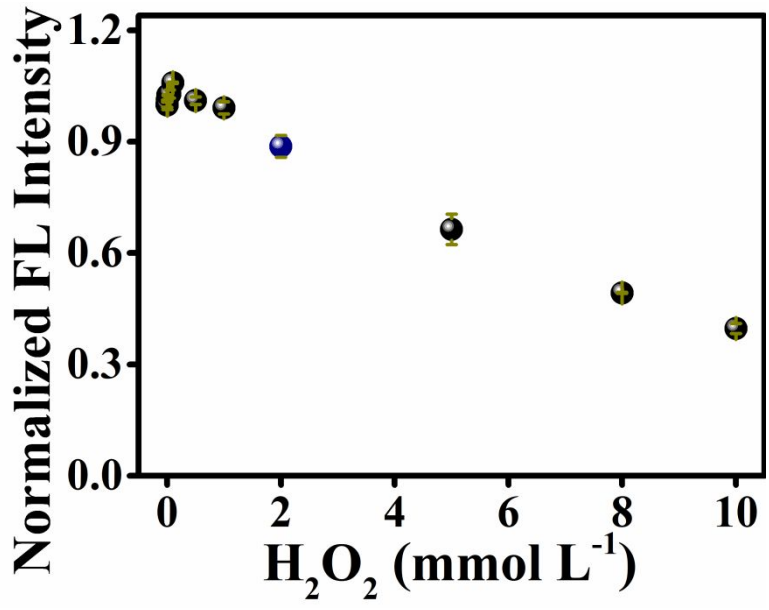

Figure S8. The stability of CDs in the presence of 0-10 mmol L^{-1} H_2O_2.

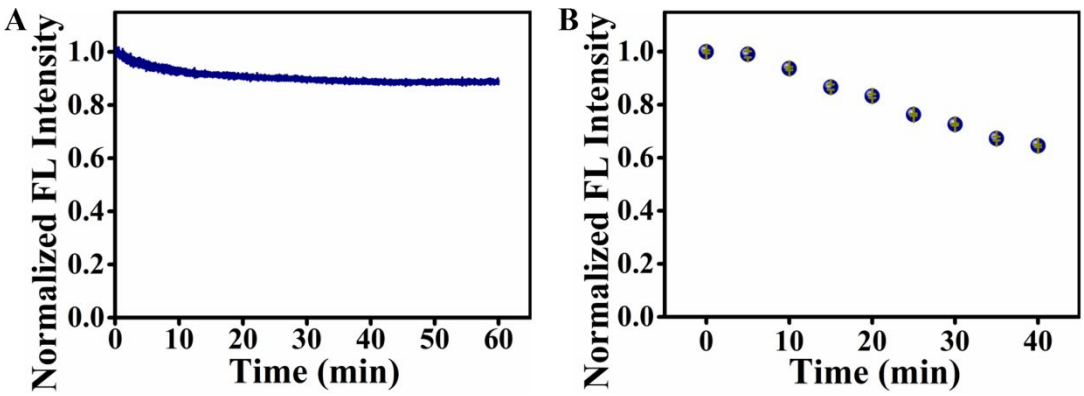

Figure S9. Photostability of CDs. (A) Time course scan curve obtained by 555 nm continuously exciting for 60 min. (B) Normalized FL intensity obtained by intensive xenon lamp continuous irradiation (17 W/cm^2) for 40 min.

Characterization of CoOOH Nanosheets

The CoOOH nanosheets were characterized through TEM, AFM, XRD, XPS, and FT-IR spectroscopy. TEM image revealed that the size of CoOOH nanosheets was in the range of 88 ± 8 nm and lattice spacing of 0.27 nm was observed in HRTEM image (Figure S10), corresponding to (012) plane of CoOOH nanosheets. As shown in AFM image, the mean height was around 5.6 nm (Figure S11). The XRD pattern (Figure S12) was in accord with hexagonal-like CoOOH nanosheets (JCPDS no.07-0169) as the literature reported. In the FT-IR spectrum (Figure S13), characteristic peaks for O-H stretching vibration at 3300 cm^{-1}, Co–O double bond vibration at 1640 cm^{-1} and Co-O^{2-} complex vibration at 569 cm^{-1} were seen. The XPS spectra (Figure S14) of CoOOH nanosheets exhibited two peaks centered at 794 eV and 779 eV, which were assigned to Co $2p_{1/2}$ and Co $2p_{3/2}$, respectively.

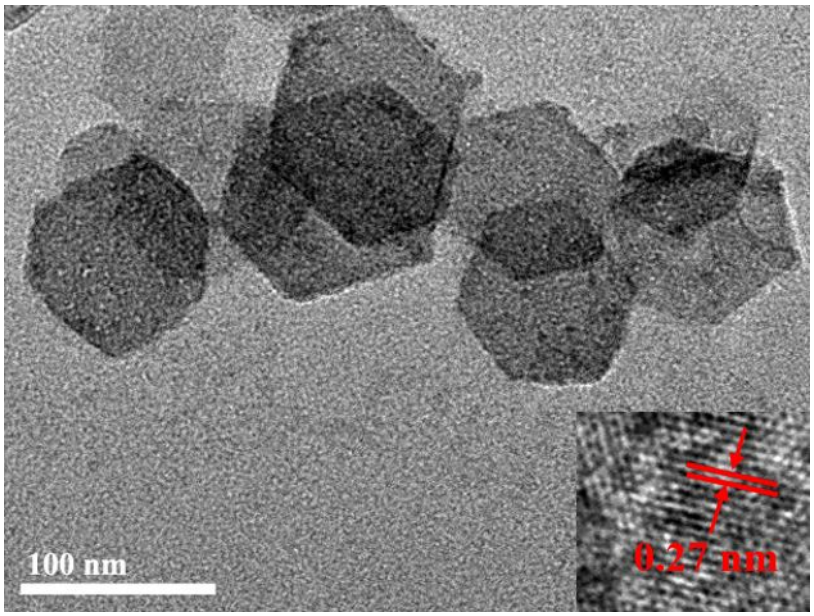

Figure S10. TEM image and HRTEM image (insert) of CoOOH nanosheets.

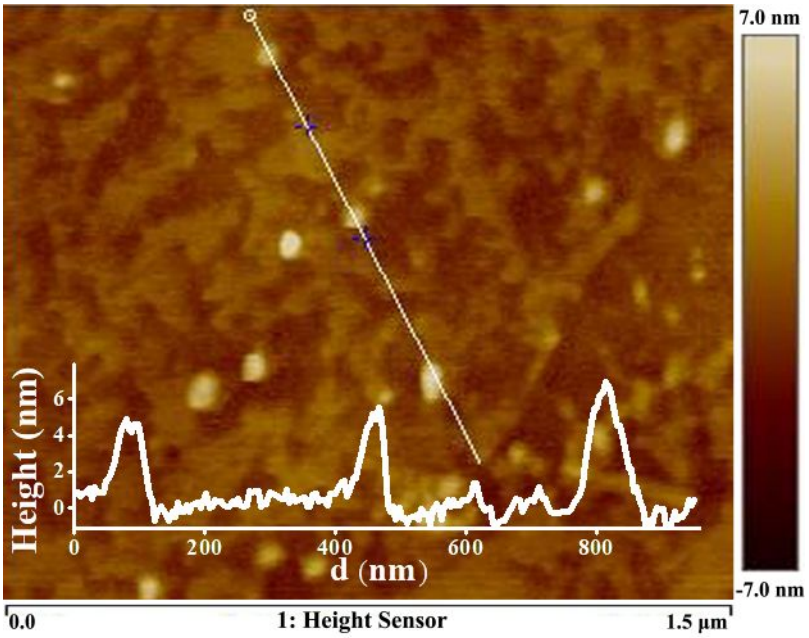

Figure S11. AFM image of CoOOH nanosheets.

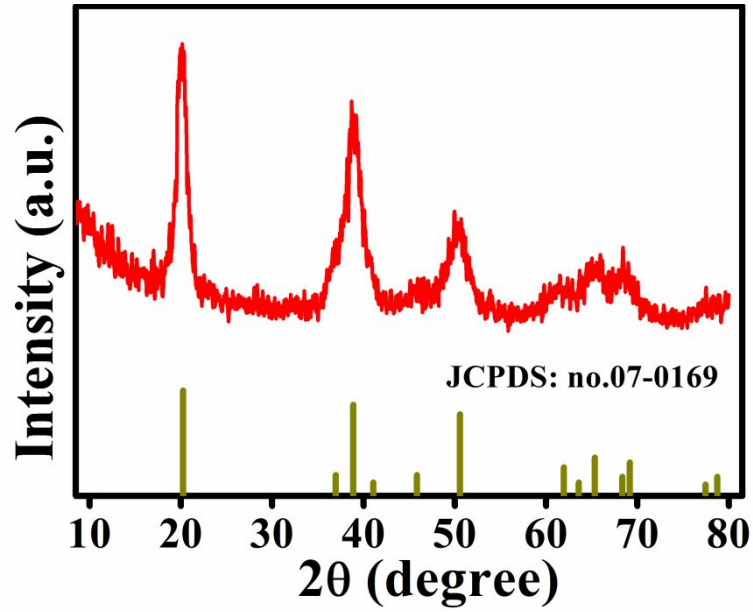

Figure S12. XRD pattern of CoOOH nanosheets.

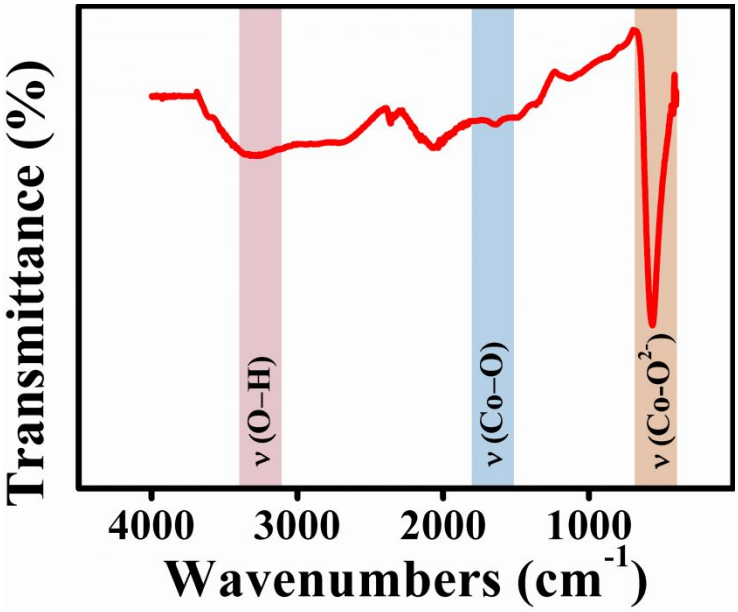

Figure S13. FT-IR spectrum of CoOOH nanosheets.

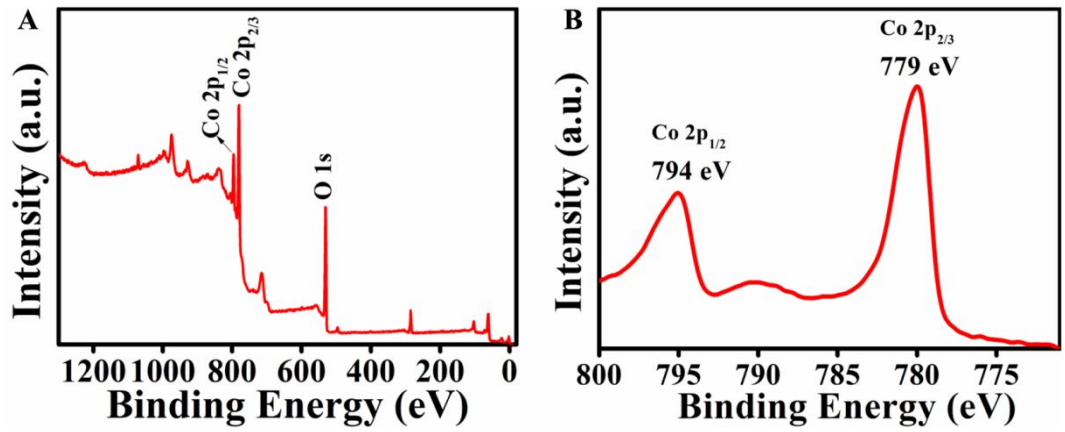

Figure S14. XPS (A) and high-resolution Co 2p (B) spectra of CoOOH nanosheets.

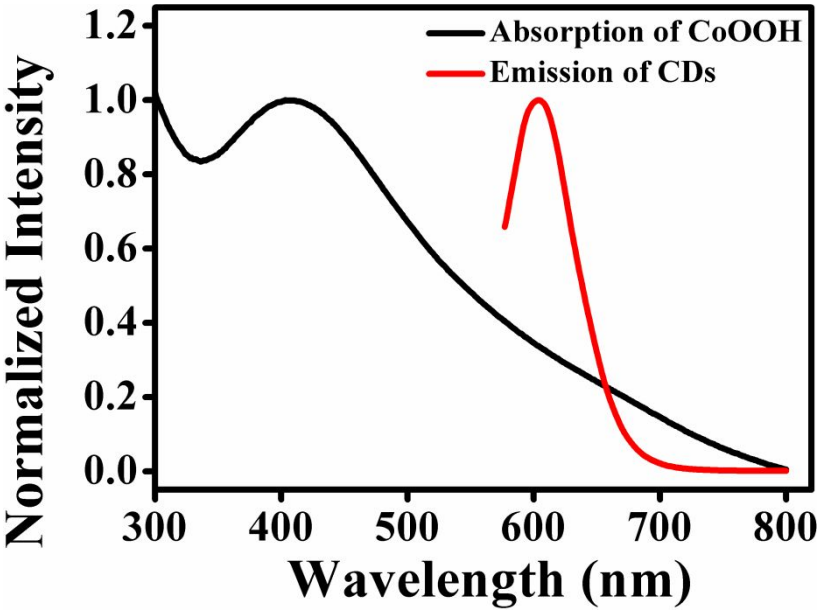

Figure S15. UV-vis spectrum of CoOOH nanosheets and FL emission spectrum of CDs.

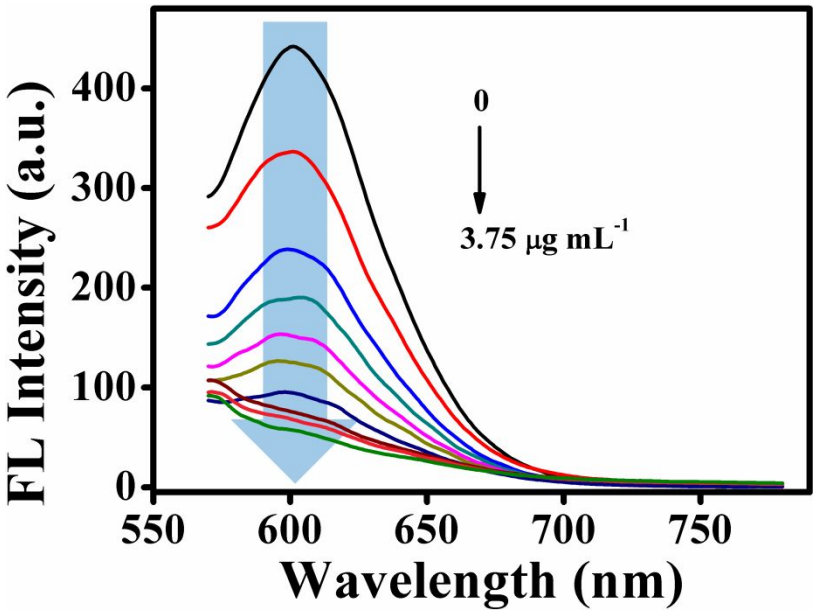

Figure S16. FL spectra with various concentrations of CoOOH nanosheets

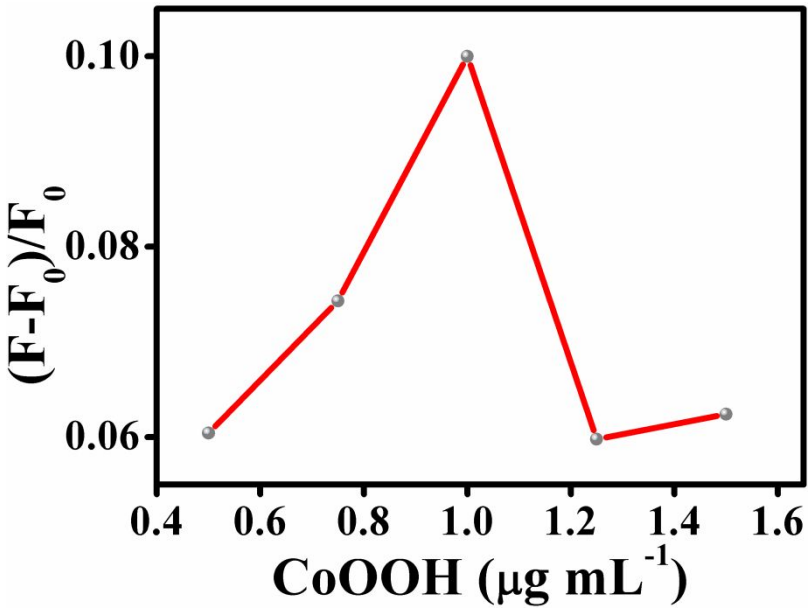

Figure S17. Effect of the concentration of CoOOH nanosheets on AA assay.

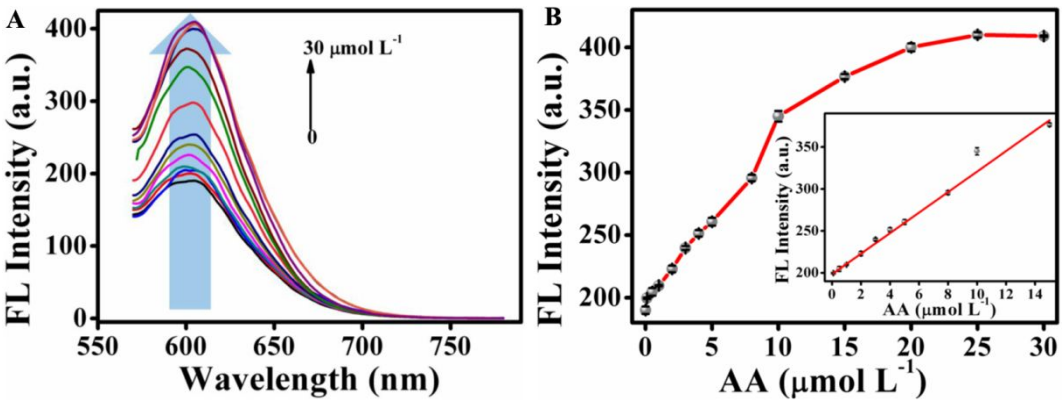

Figure S18. (A) FL spectra with various concentrations of AA. (B) FL intensity versus the concentration of AA. Inset: linear relationship between FL intensity and the concentration of AA.

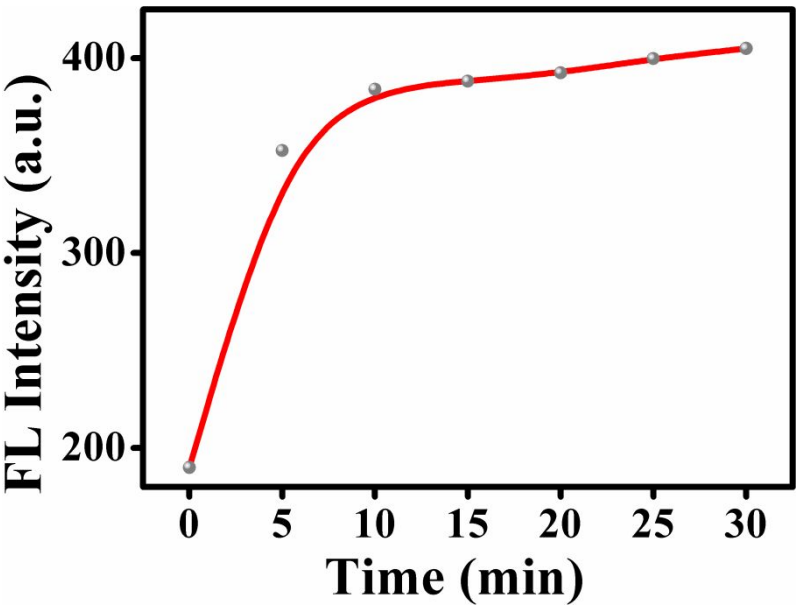

Figure S19. Effect of reaction time between ALP and AAP on ALP assay.

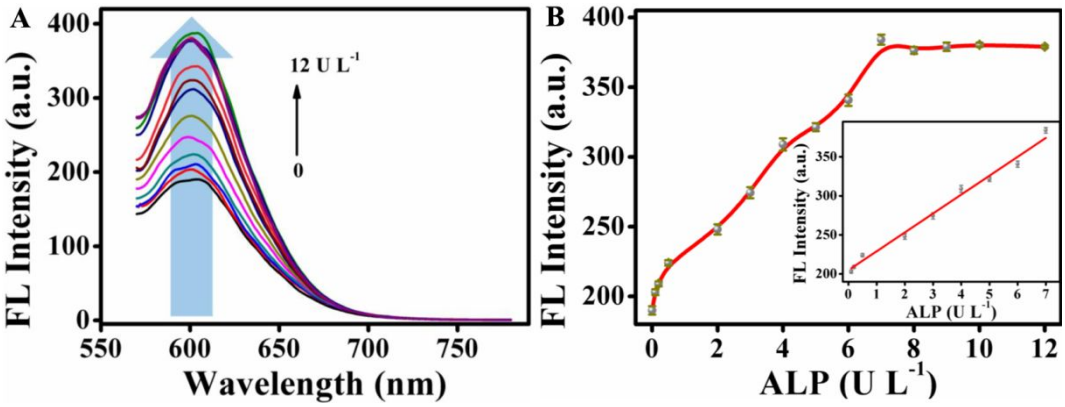

Figure S20. (A) FL spectra with various concentrations of ALP. (B) FL intensity versus the concentration of ALP. Inset: linear relationship between FL intensity and the concentration of ALP.

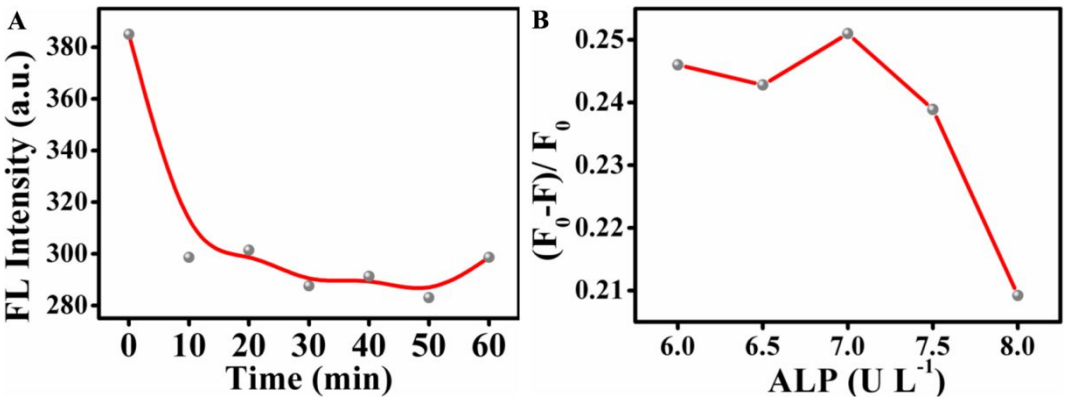

Figure S21. (A) Effect of reaction time between 2, 4-D and ALP on 2, 4-D assay; (B) Effect of ALP concentration on 2, 4-D assay (F and F_0 correspond to the fluorescence intensity in the presence and absence of 2, 4-D, respectively).

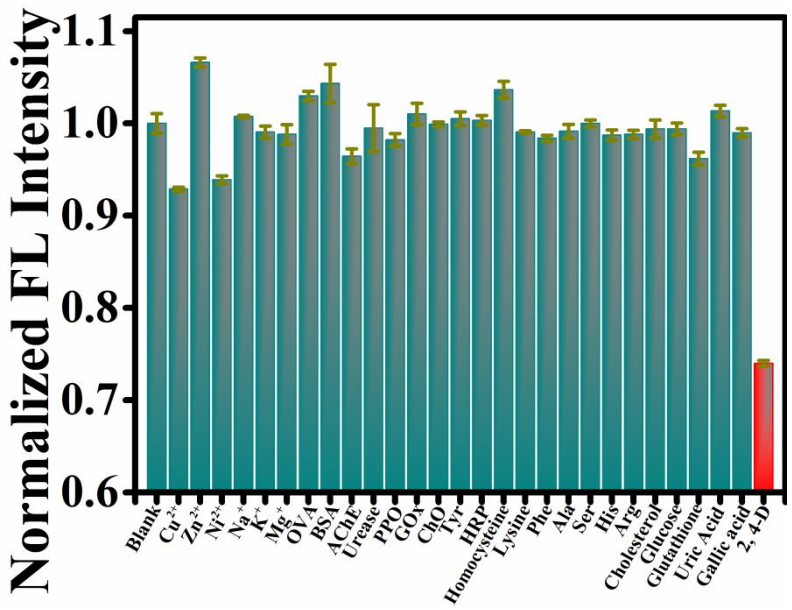

Figure S22. Selectivity performance studies toward some common substances with the same concentration (10.0 mg L^{-1}), including Cu^{2+}, Zn^{2+}, Ni^{2+}, Na^{+}, K^{+}, Mg^{2+}, ovalbumin (OVA), bovine serum albumin (BSA), acetylcholinesterase (AChE), urease, polyphenol oxidase (PPO), glucose oxidase (GOx), choline oxidase (ChO), tyrosinase (Tyr), horse radish peroxidase (HRP), homocysteine, lysine, phenylalanine (Phe), alanine (Ala), serine (Ser), histidine (His), arginine (Arg), cholesterol, glucose, glutathione, uric acid, gallic acid.

Figure S23. Actual device design of smartphone fluorometric sensing platform.

Design of Smartphone App

Red FL emission signals of CDs/CoOOH probe were captured by the smartphone CMOS sensor under the control of FCSMP. We selected the (1353, 2041) pixel dot as the symmetry center, and a 125 × 125 pixels rectangular region was chosen in the collected RGB image, which could recognize chromaticity value of images in red, green, and blue channels. Finally, 25 pixels dots were selected, the distance between each pixel dot was 5 pixels. Afterwards, App performed the transformation from the RGB value to gray value to investigate the relationship between smartphone readout gray value and the concentration of analysis target. What FCSMP does was to convert optical signals into digital signals, that is to say, collected images could be precisely transformed into corresponding concentration for output.

As exhibited in Figure S20, FCSMP with a user-friendly interface primarily could realize three functions. The first part was employed for information extraction and analysis. Once the user clicked into the "Photo" interface, smartphone camera would take a picture of the test sample. When we performed "Analysis" operation after five seconds, and the concentration of the sample to be measured would be read out on the smartphone interface. Meanwhile, the concentration of 0.5 ppm was taken as the limit to estimate whether sample content of 2, 4-D exceeded the standard concentration value. By retrieving the pictures from smartphone album, the second function was used to analyze the sample images that have acquired. Once the "File" button was executed, it would turn into the "Camera" interface and "Analysis" function was performed after manually selecting the sample picture under detection. Afterwards, the App worked as functions "Photo" to carried out sample content analysis and evaluation. The third part offered the related application instructions like copyright, responsibility, etc.

Figure S24. User interface design of smartphone App.

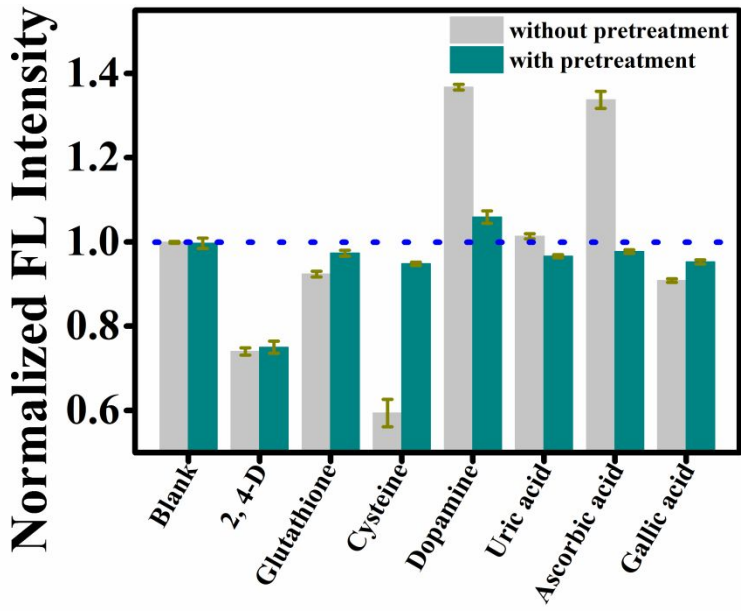

Figure S25. Selectivity performance studies with and without sample pretreatment.

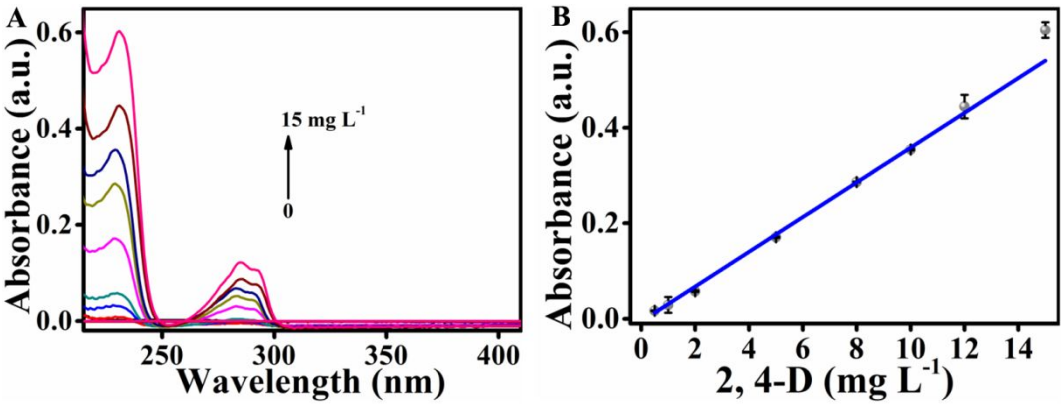

Figure S26. UV-vis-based method for 2, 4-D analysis.

Table S1. Comparison of various method for 2, 4-D detection.

Methods	Linear range (mg L^{-1})	LOD (μg L^{-1})	Assay time	Ref.
HPLC	0.1-100	-	60 min	[1]
HPLC	0.4-50	100	>70 min	[2]
Electrochemistry	0.1-1	50	~7 min	[3]
Photoelectrochemistry	0.00005-0.05	0.05	7 h	[4]
Photoelectrochemistry	0.110-2.763	2.2	~20 min	[5]
Colorimetry	0.1-100	20	>70 min	[6]
ELISA	0.001-0.35	0.079	>24 h	[7]
ELISA	0.0001-0.33	0.072	2.5 h	[8]
Fluorometry	0.05-1000	15	>20 min	[9]
Fluorometry	0.05-15	11.6	30 min	This work

REFERENCES

(1) Zhou, C.; Li, H.; Zhou, H.; Wang, H.; Yang, P.; Zhong, S. Water-compatible halloysite-imprinted polymer by Pickering emulsion polymerization for the selective recognition of herbicides. *J. Sep. Sci.* **2015**, *38*, 1365-1371.

(2) Yang, W.; Jiao, F.; Zhou, L.; Chen, X.; Jiang, X. Molecularly imprinted polymers coated on multi-walled carbon nanotubes through a simple indirect method for the determination of 2, 4-dichlorophenoxyacetic acid in environmental water. *Appl. Surf. Sci.* **2013**, *284*, 692-699.

(3) Arduini, F.; Cinti, S.; Caratelli, V.; Amendola, L.; Palleschi, G.; Moscone, D. Origami multiple paper-based electrochemical biosensors for pesticide detection. *Biosens. Bioelectron.* **2019**, *126*, 346-354.

(4) Zhao, W. W.; Ma, Z. Y.; Xu, J. J.; Chen, H. Y. In situ modification of a semiconductor surface by an enzymatic process: A general strategy for photoelectrochemical bioanalysis. *Anal. Chem.* **2013**, *85*, 8503-8506.

(5) Shi, H.; Zhao, G.; Liu, M.; Zhu, Z. A novel photoelectrochemical sensor based on molecularly imprinted polymer modified TiO_2 nanotubes and its highly selective detection of 2, 4-dichlorophenoxyacetic acid. *Electrochem. Commun.* **2011**, *13*, 1404-1407.

(6) Jin, L. Y.; Dong, Y. M.; Wu, X. M.; Cao, G. X.; Wang, G. L. Versatile and amplified biosensing through enzymatic cascade reaction by coupling alkaline phosphatase in situ generation of photoresponsive nanozyme. *Anal. Chem.* **2015**, *87*, 10429-10436.

(7) Wang, Q.-L.; Li, J.; Li, X.-D.; Ding, L.-S.; Xie, J.; Qing, L.-S. A simple nano-SiO_2-based ELISA method for residue detection of 2, 4-dichlorophenoxyacetic acid in bean sprouts. *Food Anal. Methods* **2016**, *10*, 1500-1506.

(8) Deng, A.-P.; Yang, H. A multichannel electrochemical detector coupled with an ELISA microtiter plate for the immunoassay of 2, 4-dichlorophenoxyacetic acid. *Sens. Actuators, B* **2007**, *124*, 202-208.

(9) Hu, X. L.; Wu, X. M.; Fang, X.; Li, Z. J.; Wang, G. L. Switchable fluorescence of gold nanoclusters for probing the activity of alkaline phosphatase and its application in immunoassay. *Biosens. Bioelectron.* **2016**, *77*, 666-672.